

Article

Polarization-Insensitive Metasurface for Harvesting Electromagnetic Energy with High Efficiency and Frequency Stability over Wide Range of Incidence Angles

Fan Yu ¹, Guo-Qiang He ^{1,2,*}, Xue-Xia Yang ^{1,*}, Jinxin Du ¹  and Steven Gao ³

¹ Key Laboratory of Specialty Fiber Optics and Optical Access Networks, Joint International Research Laboratory of Specialty Fiber Optics and Advanced Communication, Shanghai Institute of Advanced Communication and Data Science, Shanghai University, Shanghai 200444, China; yufan1994@shu.edu.cn (F.Y.); Jinxin_du@shu.edu.cn (J.D.)

² Department of Electronics and Informatics, Vrije Universiteit Brussel, 1050 Ixelles, Belgium

³ School of Engineering and Digital Arts, University of Kent, Canterbury CT2 7NZ, UK; s.gao@kent.ac.uk

* Correspondence: ghe@shu.edu.cn (G.-Q.H.); yang.xx@shu.edu.cn (X.-X.Y.)

Received: 9 October 2020; Accepted: 9 November 2020; Published: 13 November 2020



Abstract: In this paper, a polarization-insensitive metasurface, harvesting electromagnetic (EM) energy with high efficiency and frequency stability over a wide range of incidence angles, is proposed. The previously reported metasurfaces suffer from their maximum efficiencies shifting with the frequency when the incidence angle increases. By introducing a square-shaped metal via ring around the elements, the mutual coupling among adjacent cells is reduced so that the proposed metasurface can maintain maximum efficiency at the fixed operation frequency over a wide range of incidence angles. Furthermore, with one single harvesting via in the proper position for the connection of a harvesting load, the metasurface can collect EM energy effectively with both transverse electric (TE) and transverse magnetic (TM) polarizations in one single harvesting load. Compared with the reported metasurfaces, this proposed metasurface has a higher efficiency and fixed operation frequency within a wide incidence range. The energy distribution, harvesting efficiency, and surface current are simulated to investigate the operation mechanism of the proposed metasurface. The simulation results show that the maximum harvesting efficiency is 91% at 5.8 GHz for both TE and TM polarizations at the normal incidence. When the incident angle increases to 75°, the maximum efficiency is achieved at 5.79 GHz (0.19% shift), and the maximum efficiencies of TM and TE polarizations are 91% and 68%, respectively. A 5 × 5 array is fabricated and tested. The experimental results are in good agreement with the simulated ones.

Keywords: electromagnetic energy harvesting; metasurface; frequency stability; polarization-insensitive

1. Introduction

With the rapid development of various wireless communications, the environment is filled with more and more electromagnetic (EM) waves, which makes harvesting the ambient EM energy become possible. The environmental EM wave varies with the frequency, incidence angle, and polarization. The conventional rectenna, composed of a receiving antenna and a rectifier circuit, usually operates at a pre-defined incidence angle, polarization, and frequency [1,2]. Therefore, they are not sufficient for harvesting ambient EM energy. The metasurface, a periodic array of metamaterial cells with a thin substrate [3], has been applied for designing absorbers [4–8], improving the performance of antennae [9–11], and so on. The absorber absorbs the EM energy and dissipates it in the substrate

without reflection. Meanwhile, the harvester should not only receive EM waves, but also effectively transfer the energy to a harvesting load for further energy recycling. Compared with the conventional rectenna, the harvester could receive EM waves with a higher efficiency over a wide range of incidence angles.

In 2012, Ramahi et al. proposed harvesting EM energy by the metasurface first [12]. Afterward, the research on metasurfaces was mainly based on split-ring resonators (SRRs) [12,13] and complementary split-ring resonators (CSRRs) [14,15], and metasurfaces with the characteristics of a wide range of incidence angles [16–20], broadband [12,16,21], multiband [15,22], and polarization insensitivity [12–16,23,24] were investigated. There are two main methods for designing and analyzing metasurfaces: the artificial intelligence [22,25] and equivalent circuit approach [26–28]. However, there exists a defect in those metasurfaces; the harvesting efficiency decreases significantly at a fixed frequency as the incidence angle increases. That is to say, the operation frequency of the peak efficiency changes with the incidence angle, although the harvester operates on a wide angle range. A broadband metasurface can avoid the influence of frequency shifting. However, the reported broadband metasurfaces could only remain at half of the peak efficiency [12,16,21], and the band with an efficiency of 90% was maintained only around the center frequency in the broadside direction.

An absorber with a circular sector structure was proven to have a stable operation frequency under oblique incidence [10,11]. In this paper, a polarization-insensitive metasurface with frequency variation of only 0.19% and up to a 75° incidence angle is proposed. The harvesting load is introduced in the eight circular sectors at a proper position to make the metasurface insensitive to polarization, and it is applied to collect EM energy. A square, ring-shaped metal via is added around the metasurface unit cell to reduce the mutual coupling for further improvement of frequency stability. Table 1 gives a comparison of the frequency deviations of the published works, with the incidence angle range and the maximum harvesting efficiencies at the original frequency on the broadside and at a 60° incidence angle. It is obvious that the proposed metasurface can maintain a higher efficiency over a wide, oblique incidence angle at the fixed operation frequency than those previously published.

Table 1. Comparison of the frequency deviation and maximum efficiency of metasurfaces with a wide range of incidence angles.

Ref	Center Frequency	Frequency Deviation	Incidence Angle Range	Efficiency at 0°	Efficiency at 60°
[16]	5.4 GHz	300 MHz (5.55%)	0–60°	92%	48%
[17]	5.8 GHz	75 MHz (1.3%)	0–75°	88%	62%
[18]	2.7 GHz	80 MHz (2.96%)	0–60°	91%	54%
[19]	5.7 GHz	120 MHz (4.44%)	0–60°	81%	30%
[20]	3.8 GHz	100 MHz (2.63%)	0–45°	90%	52%
This work	5.8 GHz	11 MHz (0.19%)	0–75°	91%	72%

2. Design of the Harvester

As shown in Figure 1, the metasurface consisted of a metal ground, a dielectric substrate layer, and a periodic array of specially designed units. The centrally symmetrical circular sectors had the center point of O and a radius of R1. Each unit cell was surrounded by a square, ring-shaped metal via, and a metal harvesting via for connecting the harvesting load was placed near the center at position O'. This via shifted a little from the center point O and was located at the position having the strongest surface current. The polarization insensitivity property was generated from the approximate, centrally symmetrical structure (except for the harvesting via). To effectively conduct and collect the absorbed EM energy, a harvesting load of 50 Ω was added between the cell and the ground through the harvesting via. The position of the harvesting via and the value of the harvesting load were adequately optimized to maximize the harvesting efficiency of the metasurface.

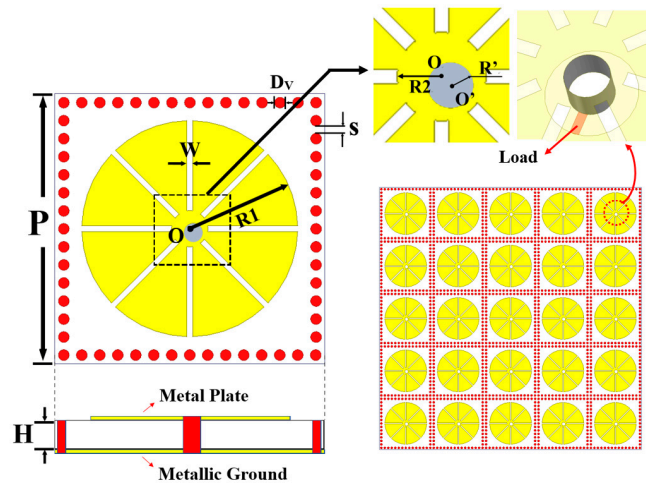


Figure 1. Topology of the proposed metasurface and unit cell structure.

The dielectric substrate had a thickness of 0.8 mm, a dielectric constant of 2.65, and a loss tangent of 0.0012. The top and bottom metal planes were copper foil, with a conductivity of 5.8×10^7 S/m and a thickness of 0.035 mm. The dimensions of the unit cell were as follows: $R1 = 5.8$ mm, $R2 = 1$ mm, $R' = 0.6$ mm, $W = 0.3$ mm, $Dv = 0.6$ mm, $S = 0.6$ mm, $H = 0.8$ mm, and $P = 15$ mm.

3. Results and Analysis

The harvesting efficiency is the most important index for a harvester. This work focuses on maximizing the harvesting efficiency with a wide range of incidence angles and a fixed operation frequency. The harvesting efficiency of the metasurface was calculated as $\eta = P_{\text{LOAD}}/P_{\text{INC}}$, where P_{LOAD} is the total time-average power dissipated on the loads and P_{INC} is the total time-average power incident on the metasurface. High Frequency Structure Simulator (HFSS) software was used to analyze the performance of the harvester. The periodic boundary condition was applied to the unit cell to numerically realize an infinite array. The unit cell was excited by the Floquet port with two modes of transverse electric (TE) and transverse magnetic (TM) polarizations at the top boundary. These two modes correspond to a plane wave, with the electric component perpendicular to the xz - and yz -planes, respectively.

3.1. Simulation Results

The absorbed EM energy, the energy distribution on the load, and the harvesting efficiency of the metasurface at a normal incidence were analyzed. It can be seen from Figure 2a that the metasurface had the maximum absorption efficiency at 5.8 GHz. The absorption and harvesting efficiencies were 96% and 91%, respectively. Only 5% of the energy was dissipated in the substrate and metal, and most of the energy was harvested by the resistor, which indicates that the metasurface can effectively collect EM energy. Figure 2b shows the harvesting efficiency of the TE and TM polarizations, which were basically the same. The arbitrary polarization wave could be deconstructed into two orthogonal polarizations of TE and TM waves so that a similar efficiency would be obtained for an arbitrary polarization at the normal incidence. Thus, the metasurface was insensitive in polarization. As shown in Figure 2c, the harvester performed well with low cross polarization, measuring below -20 dB at 5.8 GHz, which means the energy could be harvested simultaneously and separately by these two orthogonal polarizations.

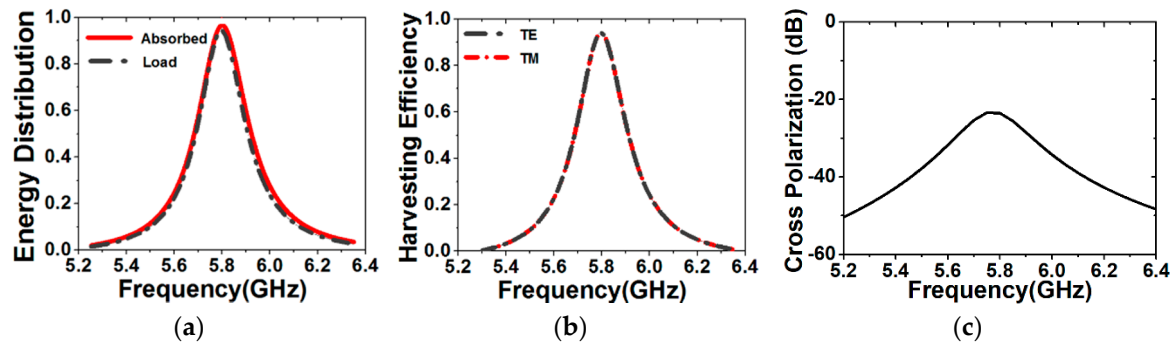


Figure 2. (a) Energy distribution efficiency versus frequency. (b) Harvesting efficiency versus frequency for transverse electric (TE) and transverse magnetic (TM) polarized waves at the normal incidence. (c) Cross polarization versus frequency.

The absorption principle can be explained by the impedance matching between the free space and the metasurface interface. The effective parameters were extracted from the complex scattering parameters by the standard retrieval procedure [3]. As shown in Figure 3, the extracted permittivity and permeability at the resonance frequency were $(4.42-j63.4)$ and $(4.44-j44.60)$, respectively. The normalized impedance ($z = \sqrt{\mu/\epsilon}$), compared with that of the free space (377Ω), was $(0.84-j0.01) \Omega$. Thus, the metasurface was a good match with the free space, and reflections at the metamaterial interface would be very small.

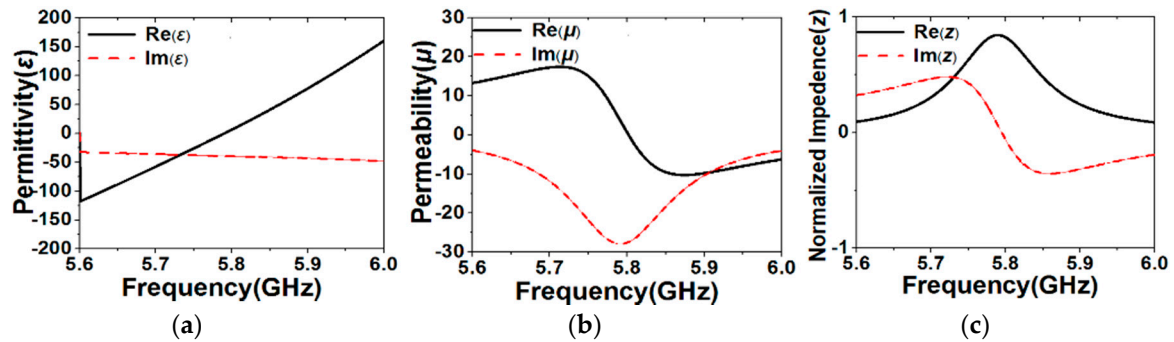


Figure 3. Extracted effective material parameters of (a) permittivity, (b) permeability, and (c) impedance.

The operation mechanism of the metasurface can be analyzed by the equivalent circuit approach. The transmission line equivalent circuit of the proposed metasurface is shown in Figure 4. Part 1 represents the incident plane wave from the free space, which had a wave impedance of 377Ω . Part 2 is for the metasurface. C_1 and L_1 represent the total capacitance between each of two sectors and the total inductance of the eight sectors, respectively. C_2 and L_2 represent the capacitance between the unit pattern and the metallic ground and the inductance of the metal via near the center, respectively. R is the harvesting load, and C_3 represents the capacitance between the via and the ground. The substrate between the unit pattern and the ground can be modeled as a transmission line, with a characteristic impedance of $377/\sqrt{\epsilon_r} = 231 \Omega$.

The value of each lumped element in the equivalent circuit could be estimated using a microstrip line model that estimates the total inductance and capacitance [29]. Optimized using Advanced Design System (ADS) software, the reflection coefficient of the equivalent circuit, with a comparison to that of the metasurface in HFSS, is shown in Figure 5a. The resonance frequencies of the two models both occurred at 5.8 GHz, which agrees well with the experiment results. Figure 5b,c show the trend of the reflection coefficient changing with the value of R . The minimum reflection was achieved with a value of 50, and the reflection increased when the value shifted from 50 in both models. The similar trend further demonstrates the consistency of the two models. It should be noticed that the coupling effects

in the HFSS model were much more complicated than those in the equivalent circuit, which caused the slight difference between the results of the two models.

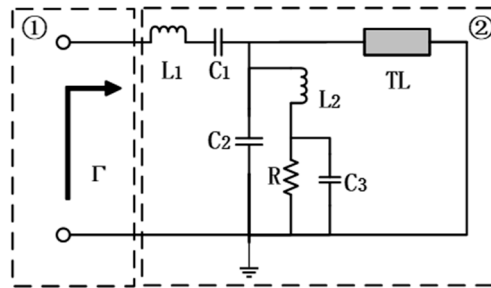


Figure 4. Equivalent circuit model of the proposed metasurface. The parameters of the elements are as follows: $L_1 = 0.2 \text{ nH}$, $C_1 = 1.6 \text{ pF}$, $L_2 = 0.1 \text{ nH}$, $C_2 = 2.6 \text{ pF}$, $C_3 = 1.2 \text{ pF}$, and $R = 50 \Omega$.

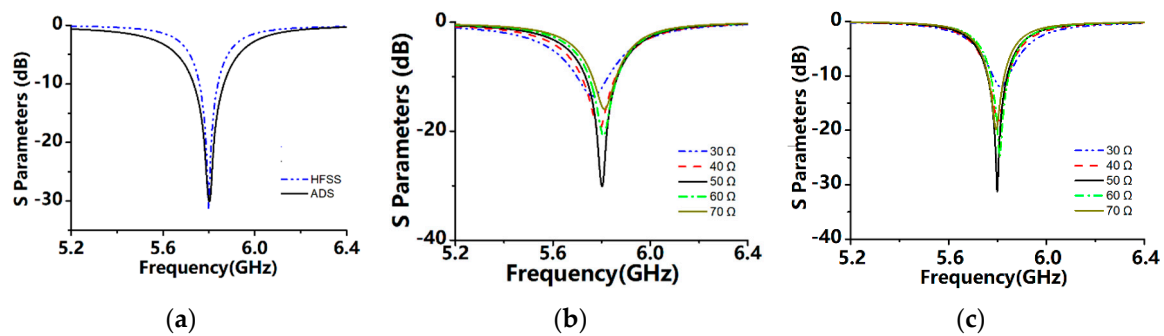


Figure 5. (a) Reflection coefficient of the equivalent circuit in Advanced Design System (ADS), compared with that of the metasurface in HFSS. (b) Reflection coefficient, changing with the value of R in ADS. (c) Reflection coefficient, changing with the value of R in HFSS.

To analyze the polarization insensitivity feature, the surface current of the metasurface unit cell was explored. Figure 6a shows the current distribution of the TE wave at the normal incidence, and Figure 6b–d show the surface current with the polarization plane being rotated by 30° , 60° , and 90° along the xoy-plane, respectively. For any polarization angle, the current always passed through the circle in the center, and the harvesting load was placed at the concentrated point of the current, which was the criterion of determining the harvesting load position. What is more, the current distribution density and pattern stayed relatively unchanged, due to the approximate symmetrical pattern of the unit. Therefore, the unit cell could effectively harvest the energy and maintain a high efficiency for arbitrary polarization waves at the normal incidence.

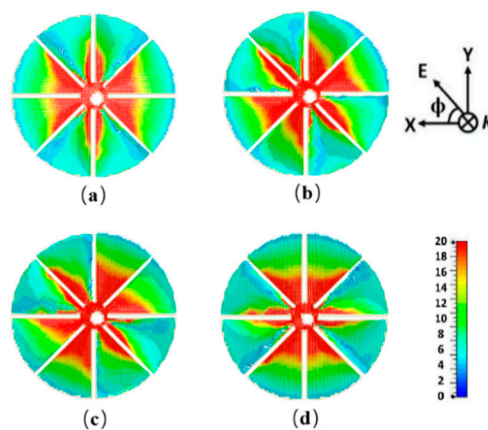


Figure 6. Surface current on metal of the unit cell at the normal incidence for different polarization angles. (a) $\varphi = 0^\circ$, (b) $\varphi = 30^\circ$, (c) $\varphi = 60^\circ$, and (d) $\varphi = 90^\circ$.

The harvesting efficiency of the metasurface under an oblique incidence for TE and TM polarizations was studied. Figure 7a shows the efficiency for TE polarization. As the incidence angle increased from 0° to 75° , the operation frequency in the broadside direction was nearly unchanged, and the harvesting efficiency reduced gradually. When the incident angle increased to 60° , the harvesting efficiency was 72%. For TM polarization, as the incidence angle increased from 0° to 75° , the operation frequency in the broadside direction shifted by only 11 MHz. When the incidence angle was 60° , the harvesting efficiency was 91%, as shown in Figure 7b. The simulated results show that the metasurface can maintain a high efficiency at a fixed frequency over a wide range of incidence angles, and it remains insensitive to polarization, even in the case of an oblique incidence under 45° .

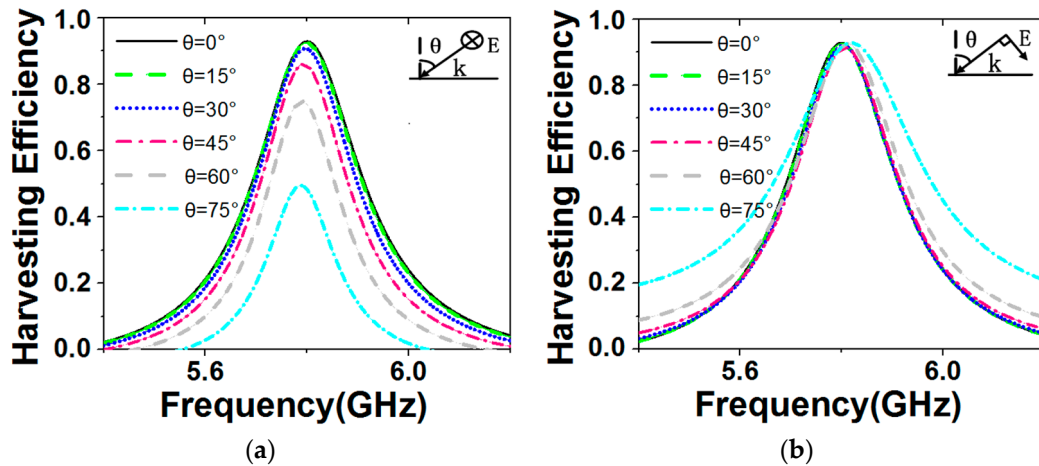


Figure 7. Simulated harvesting efficiency of the infinite metasurface under different incidence angles for (a) TE and (b) TM polarized incident waves.

In this design, a square-shaped metal via ring around the unit cells is proposed to decrease the mutual coupling and improve the frequency stability. Figure 8 shows the impedance for TM polarization versus the frequency with and without the square rings when the incident angles are different. It can be observed that the relative impedance shifts with the frequency as the incident angle increasing. When the incidence angle increases from 0° to 75° , the frequencies shift 15 MHz and 48 MHz with and without the square rings, respectively.

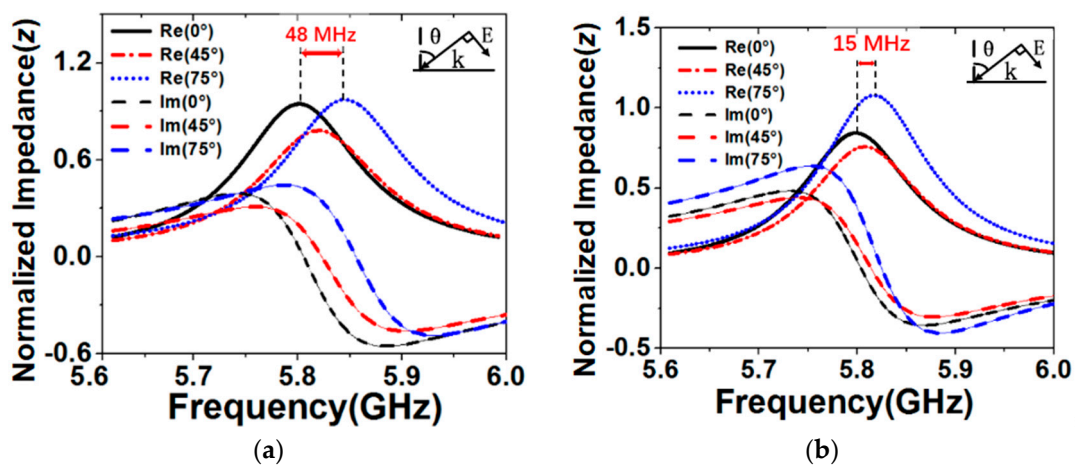


Figure 8. The impedance (a) without, (b) with square-shaped metal via rings.

The variation tendency of the harvesting efficiency is similar to that of the impedance for TM polarization as shown in Figure 9. Without the square rings, the operation frequency at the broadside direction shifts 48 MHz when the incidence angle increase from 0° to 75° . With the square rings,

the operation frequency at the broadside direction shifts only 11 MHz, which makes the efficiency at the original operation frequency of 5.8 GHz 10% higher.

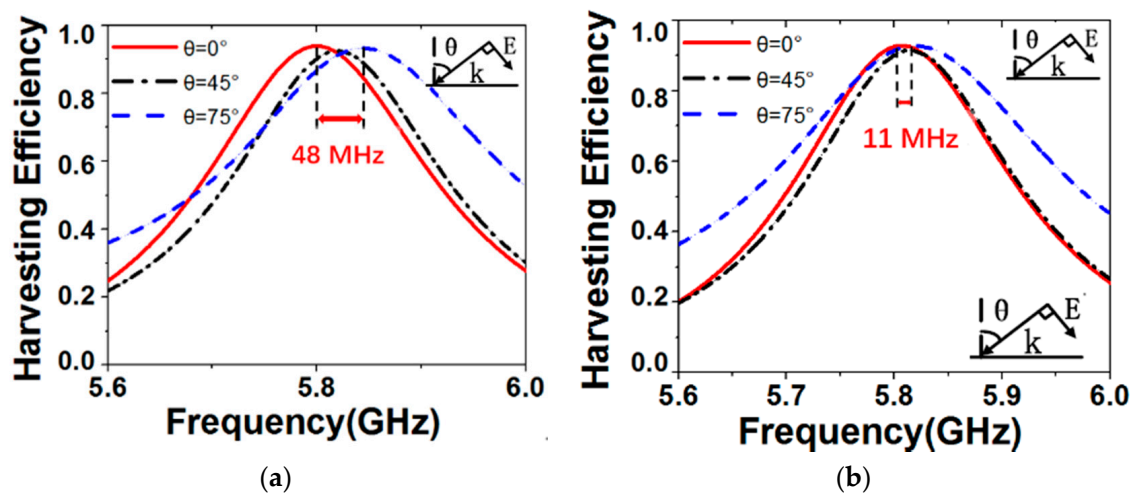


Figure 9. The harvesting efficiencies (a) without, (b) with square-shaped metal via rings.

3.2. Measurement Results

To experimentally validate the energy harvesting efficiency of this metasurface, we fabricated a 5×5 array, as shown in Figure 10a,b. A horn antenna was fed by a signal generator and illuminated the metasurface with a distance of R . Power was delivered to the central unit cell and measured by the power meter. The far field distance of R was defined according to the aperture of the horn. The experiment setup is shown in Figure 10c.

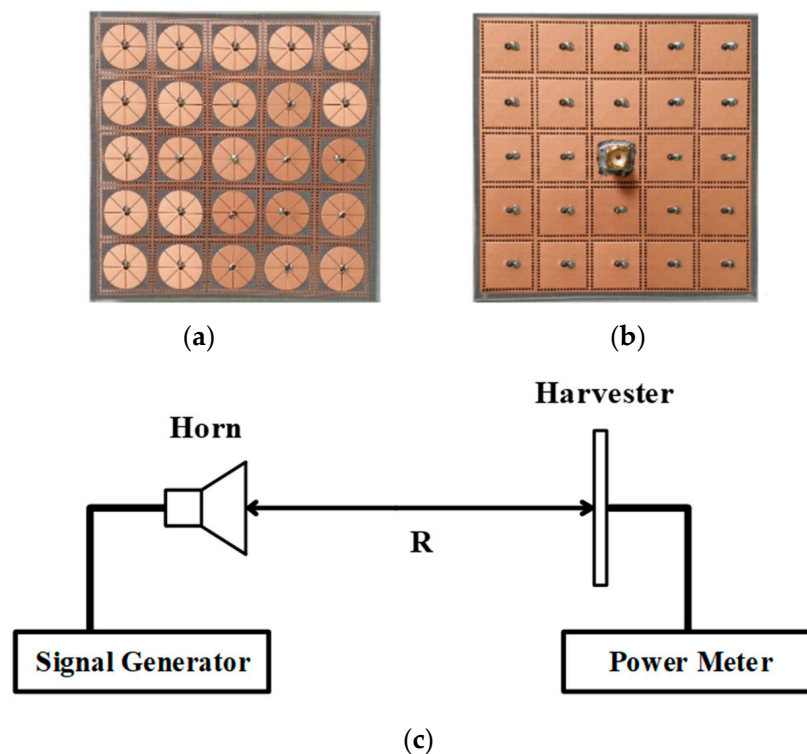


Figure 10. A photograph of the 5×5 array from (a) the top and (b) the bottom. (c) The schematic diagram of the measurement setup used in the experiment.

The incident power was calculated by multiplying the incident power intensity and the physical area of the central unit. The incident power intensity S at the distance of R from the horn was calculated using the following equation [16]:

$$\vec{S} = \hat{r} \frac{GP_{IN}}{4\pi R^2} \quad (1)$$

where P_{IN} is the input power and G is the gain of the horn. The reason for measuring a center unit cell is that it was the closest to the one in the infinite array. In order to achieve an EM coupling environment similar to the one in the simulation, the other unit ports of the array were all connected to a 50Ω load (see Figure 10b).

To adjust the incidence angle in the experiments, we rotated the metasurface while keeping the transmitting horn fixed. The center point of the metasurface was aligned to that of the horn plane. Figure 11 shows the measured harvesting efficiency of the TE and TM waves under oblique incident angles. The maximum efficiency at the normal incidence was 88% at 5.91 GHz, which had a slight shift of 1.9% to the simulated 5.8 GHz. Compared with the original frequency of 5.91 GHz at the normal incidence, the operation frequency in the broadside direction shifted only 12 MHz (0.2%) up to a 75° incidence angle for both the TE and TM waves. When the incidence angle was 60° , the maximum harvesting efficiency was 60%. The differences between the simulated and measured results come from three aspects. Firstly, the fabricated metasurface array was 5×5 , while the simulated one was an infinite array. The finite array had the edge effect, which would influence the central cell's performance. Secondly, the simulation software imitated the infinite array by setting the period boundary condition around the unit cell, which might have caused a difference with the actual infinite array. Thirdly, the fabrication tolerances might have also induced errors. This work focused on the frequency stability over a wide range of incidence angles, and the measured results were in reasonable agreement with the simulated ones.

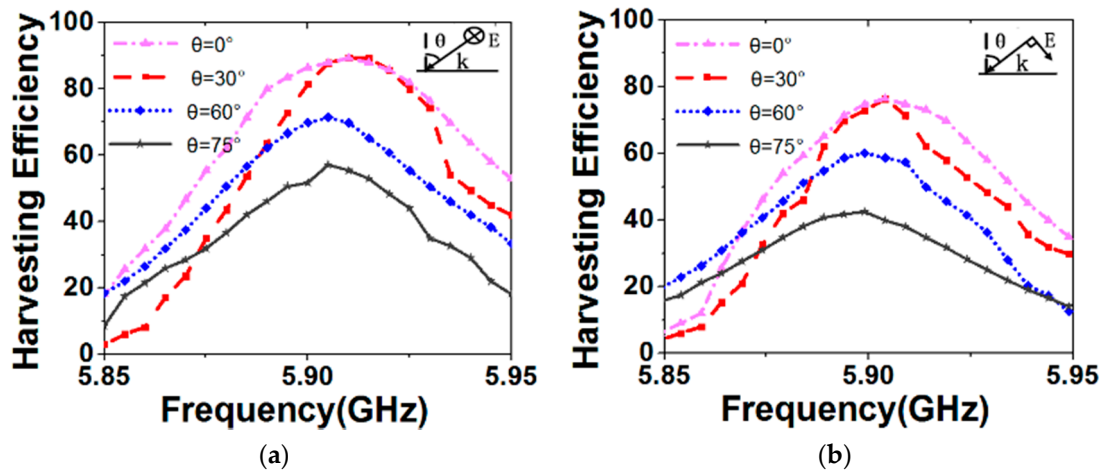


Figure 11. Measured harvesting efficiency at different incidence angles for (a) TE and (b) TM polarized incident waves.

4. Discussion

The proposed metasurface is highly efficient for harvesting EM energy in the Wireless Local Area Network (WLAN) band. The simulated and experimental results show that the metasurface has the properties of polarization insensitivity and high efficiency over a wide range of incidence angles. With square-shaped metal via rings around the unit cell and one harvesting via near the center, this metasurface solves the problem of operation frequency shifts of the maximum efficiency when the incidence angle increases. This metasurface can harvest energy with a higher efficiency over an oblique incidence in both TE and TM polarizations. This work still maintains limitations in that the efficiency decreases unequally for TE and TM polarizations when the incidence angle increases,

which could be solved in future work. Nevertheless, the metasurface can efficiently harvest complex environmental EM energy, and it is expected to be applied in wireless energy charging for low-power electronic devices.

Author Contributions: Conceptualization, F.Y.; methodology, F.Y. and G.-Q.H.; validation, F.Y.; formal analysis, F.Y.; investigation, F.Y. and G.-Q.H.; writing—original draft preparation, F.Y.; writing—review and editing, F.Y., X.-X.Y., J.D., S.G. and G.-Q.H.; supervision, X.-X.Y.; funding acquisition, X.-X.Y. All authors have read and agreed to the published version of the manuscript.

Funding: This research was funded by the National Natural Science Foundation of China, grant number 61931009.

Conflicts of Interest: The authors declare no conflict of interest.

References

1. Song, C.; Huang, Y.; Carter, P.; Zhou, J.; Joseph, S.D.; Li, G. Novel compact and broadband frequency-selectable rectennas for a wide input-power and load impedance range. *IEEE Trans. Antennas Propag.* **2018**, *66*, 3306–3316. [\[CrossRef\]](#)
2. Lin, W.W.; Ziolkowski, R.W.; Huang, J. Electrically small, low-profile, highly efficient, huygens dipole rectennas for wirelessly powering internet-of-things devices. *IEEE Trans. Antennas Propag.* **2019**, *67*, 3670–3679. [\[CrossRef\]](#)
3. Smith, D.R.; Padilla, W.J.; Vier, D.C.; Nemat-Nasser, S.C.; Schultz, S. Composite medium with simultaneously negative permeability and permittivity. *Phys. Rev. Lett.* **2000**, *84*, 4184. [\[CrossRef\]](#) [\[PubMed\]](#)
4. Landy, N.I.; Sajuyigbe, S.; Mock, J.J.; Smith, D.R.; Padilla, W.J. Perfect metamaterial absorber. *Phys. Rev. Lett.* **2008**, *100*, 207402. [\[CrossRef\]](#) [\[PubMed\]](#)
5. Bowen, L.; Vinolas, J.; Olazagoitia, J.L. Design and potential power recovery of two types of energy harvesting shock absorbers. *Energies* **2019**, *12*, 4710. [\[CrossRef\]](#)
6. Lim, D.; Lee, D.; Lim, S. Angle-and polarization-insensitive metamaterial absorber using via array. *Sci. Rep.* **2016**, *6*, 39686. [\[CrossRef\]](#)
7. Lee, D.; Hwang, J.G.; Lim, D.; Hara, T.; Lim, S. Incident angle-and polarization-insensitive metamaterial absorber using circular sectors. *Sci. Rep.* **2016**, *6*, 27155. [\[CrossRef\]](#)
8. Nguyen, T.T.; Lim, S. Wide incidence angle-insensitive metamaterial absorber for both TE and TM polarization using eight-circular-sector. *Sci. Rep.* **2017**, *7*, 3204. [\[CrossRef\]](#)
9. Lalbakhsh, A.; Afzal, M.U.; Esselle, K.P.; Smith, S.L. Low-cost nonuniform metallic lattice for rectifying aperture near-field of electromagnetic bandgap resonator antennas. *IEEE Trans. Antennas Propag.* **2020**, *68*, 3328–3335. [\[CrossRef\]](#)
10. Lou, T.; Yang, X.X.; Qiu, H.; Yin, Z.; Gao, S. Compact dual-polarized continuous transverse stub array with 2-D beam scanning. *IEEE Trans. Antennas Propag.* **2019**, *67*, 3000–3010. [\[CrossRef\]](#)
11. Lalbakhsh, A.; Afzal, M.U.; Esselle, K.P.; Smith, S.L.; Zeb, B.A. Single-dielectric wideband partially reflecting surface with variable reflection components for realization of a compact high-gain resonant cavity antenna. *IEEE Trans. Antennas Propag.* **2019**, *67*, 1916–1921. [\[CrossRef\]](#)
12. Ramahi, O.M.; Almoneef, T.S.; AlShareef, M.; Boybay, M.S. Metamaterial particles for electromagnetic energy harvesting. *Appl. Phys. Lett.* **2012**, *101*, 173903. [\[CrossRef\]](#)
13. Almoneef, T.S.; Ramahi, O.M. Metamaterial electromagnetic energy harvester with near unity efficiency. *Appl. Phys. Lett.* **2015**, *106*, 153902. [\[CrossRef\]](#)
14. Alavikia, B.; Almoneef, T.S.; Ramahi, O.M. Complementary split ring resonator arrays for electromagnetic energy harvesting. *Appl. Phys. Lett.* **2015**, *107*, 033902. [\[CrossRef\]](#)
15. Alavikia, B.; Almoneef, T.S.; Ramahi, O.M. Electromagnetic energy harvesting using complementary split-ring resonators. *Appl. Phys. Lett.* **2014**, *104*, 163903. [\[CrossRef\]](#)
16. Zhong, H.T.; Yang, X.X. Broadband meta-surface with polarization-insensitive and wide-angle for electromagnetic energy harvesting. *IWAT* **2017**, *10*, 1109.
17. Yu, F.; Yang, X.; Zhong, H.; Chu, C.; Gao, S. Polarization-insensitive wide-angle-reception metasurface with simplified structure for harvesting electromagnetic energy. *Appl. Phys. Lett.* **2018**, *113*, 123903. [\[CrossRef\]](#)
18. Ghaneizadeh, A.; Mafinezhad, K.; Joodaki, M. Design and fabrication of a 2D-isotropic flexible ultra-thin metasurface for ambient electromagnetic energy harvesting. *AIP Adv.* **2019**, *9*, 025304. [\[CrossRef\]](#)

19. Zhang, X.; Liu, H.; Li, L. Tri-band miniaturized wide-angle and polarization-insensitive metasurface for ambient energy harvesting. *Appl. Phys. Lett.* **2017**, *111*, 071902. [[CrossRef](#)]
20. Zhong, H.T.; Yang, X.X.; Song, X.T.; Guo, Z.Y.; Yu, F. Wideband metamaterial array with polarization-independent and wide incident angle for harvesting ambient electromagnetic energy and wireless power transfer. *Appl. Phys. Lett.* **2017**, *111*, 213902. [[CrossRef](#)]
21. Zhong, H.T.; Yang, X.X.; Tan, C.; Yu, K. Triple-band polarization-insensitive and wide-angle metamaterial array for electromagnetic energy harvesting. *Appl. Phys. Lett.* **2016**, *109*, 253904. [[CrossRef](#)]
22. Ghaderi, B.; Nayyeri, V.; Soleimani, M.; Ramahi, O.M. Pixelated metasurface for dual-band and multi-polarization electromagnetic energy harvesting. *Sci. Rep.* **2018**, *8*, 13227. [[CrossRef](#)] [[PubMed](#)]
23. Zhang, X.; Liu, H.; Li, L. Electromagnetic power harvester using wide-angle and polarization-insensitive metasurfaces. *Appl. Sci.* **2018**, *8*, 497. [[CrossRef](#)]
24. Zhang, P.; Li, L.; Zhang, X.; Liu, H.; Shi, Y. Design, measurement and analysis of near-field focusing reflective metasurface for dual-polarization and multi-focus wireless power transfer. *IEEE Access* **2019**, *7*, 110387–110399. [[CrossRef](#)]
25. Lalbakhsh, A.; Afzal, M.U.; Esselle, K.P. Multiobjective particle swarm optimization to design a time-delay equalizer metasurface for an electromagnetic band-gap resonator antenna. *IEEE Antennas Wirel. Propag. Lett.* **2016**, *16*, 912–915. [[CrossRef](#)]
26. Munk, B.A. *Frequency Selective Surfaces: Theory and Design*; John Wiley & Sons: Hoboken, NJ, USA, 2005.
27. Kundu, D.; Mohan, A.; Chakrabarty, A. Thickness reduction of single layer circuit analog absorber. In Proceedings of the 2015 IEEE Applied Electromagnetics Conference (AEMC), Guwahati, India, 18–21 December 2015; pp. 1–2.
28. Shang, Y.; Shen, Z.; Xiao, S. On the design of single-layer circuit analog absorber using double-square-loop array. *IEEE Trans. Antennas Propag.* **2013**, *61*, 6022–6029. [[CrossRef](#)]
29. Marcuvitz, N. *Waveguide Handbook*; IET: Edison, NJ, USA, 1951; Volume 21.

Publisher's Note: MDPI stays neutral with regard to jurisdictional claims in published maps and institutional affiliations.



© 2020 by the authors. Licensee MDPI, Basel, Switzerland. This article is an open access article distributed under the terms and conditions of the Creative Commons Attribution (CC BY) license (<http://creativecommons.org/licenses/by/4.0/>).